Xenobiotica
the fate of foreign compounds in biological systems

ISSN: (Print) (Online) Journal homepage: https://www.tandfonline.com/loi/ixen20

Pharmacokinetics, metabolism and off-target effects in the rat of 8-[(1H- benzotriazol-1-yl)amino]octanoic acid, a selective inhibitor of human cytochrome P450 4Z1: β-oxidation as a potential augmenting pathway for inhibition

John P. Kowalski, Robert D. Pelletier, Matthew G. McDonald, Edward J. Kelly & Allan E. Rettie

To cite this article: John P. Kowalski, Robert D. Pelletier, Matthew G. McDonald, Edward J. Kelly & Allan E. Rettie (2021) Pharmacokinetics, metabolism and off-target effects in the rat of 8-[(1H- benzotriazol-1-yl)amino]octanoic acid, a selective inhibitor of human cytochrome P450 4Z1: β-oxidation as a potential augmenting pathway for inhibition, Xenobiotica, 51:8, 901-915, DOI: 10.1080/00498254.2021.1930281

To link to this article: https://doi.org/10.1080/00498254.2021.1930281

XENOBIOTICA
2021, VOL. 51, NO. 8, 901–915
https://doi.org/10.1080/00498254.2021.1930281

Taylor & Francis
Taylor & Francis Group

RESEARCH ARTICLE

Pharmacokinetics, metabolism and off-target effects in the rat of 8-[(1H-benzotriazol-1-yl)amino]octanoic acid, a selective inhibitor of human cytochrome P450 4Z1: β-oxidation as a potential augmenting pathway for inhibition

John P. Kowalski[a,b], Robert D. Pelletier[a], Matthew G. McDonald[a,b], Edward J. Kelly[c] and Allan E. Rettie[a]

[a]Department of Medicinal Chemistry, School of Pharmacy, University of Washington, Seattle, WA, USA; [b]Department of Drug Metabolism and Pharmacokinetics, Pfizer Boulder R&D, Boulder, CO, USA; [c]Department of Pharmaceutics, School of Pharmacy, University of Washington, Seattle, WA, USA

ABSTRACT

1. 8-[(1H-1,2,3-benzotriazol-1-yl)amino]octanoic acid (8-BOA) was recently identified as a selective and potent mechanism-based inactivator (MBI) of breast cancer-associated CYP4Z1 and exhibited favourable inhibitory activity *in vitro,* thus meriting *in vivo* characterization.
2. The pharmacokinetics and metabolism of 8-BOA in rats was examined after a single IV bolus dose of 10 mg/kg. A biphasic time-concentration profile resulted in relatively low clearance and a prolonged elimination half-life.
3. The major circulating metabolites identified in plasma were products of β-oxidation; congeners losing two and four methylene groups accounted for >50% of metabolites by peak area. The $-(CH_2)_2$ product was characterized previously as a CYP4Z1 MBI and so represents an active metabolite that may contribute to the desired pharmacological effect.
4. *Ex vivo* analysis of total CYP content in rat liver and kidney microsomes showed that off-target CYP inactivation was minimal; liver microsomal probe substrate metabolism also demonstrated low off-target inactivation. Standard clinical chemistries provided no indication of acute toxicity.
5. *In silico* simulations using the free concentration of 8-BOA in plasma suggested that the *in vivo* dose used here may effectively inactivate CYP4Z1 in a xenografted tumour.

ARTICLE HISTORY
Received 26 February 2021
Revised 8 May 2021
Accepted 10 May 2021

KEYWORDS
Cytochrome P450 4Z1; mechanism-based inhibitor; bioactivation; breast cancer; rat; fatty acid; β-oxidation; leaky hosepipe

Introduction

During their lifetime, nearly 13% of US women will be diagnosed with invasive breast cancer, which is the most prevalent form and the second leading cause of mortality for this group (DeSantis *et al.* 2019). The elucidation of new molecular drivers of this complex disease and new drugs to treat metastases are urgently needed (Capper *et al.* 2016). Cytochrome P450 4Z1 (CYP4Z1) has been identified as a mammary tissue-restricted enzyme with an unknown physiological role that is upregulated in breast cancer. Furthermore, elevated transcript levels of CYP4Z1 are frequently associated with increased tumour grade and aggressiveness (Rieger *et al.* 2004, Radvanyi *et al.* 2005, Murray *et al.* 2010, Li *et al.* 2017, Al-Esawi *et al.* 2020). Lastly, human CYP4Z1 is the only currently known functional enzyme in this subfamily (Yang *et al.* 2017).

Recently, we reported that 8-[(1H-1,2,3-benzotriazol-1-yl)amino]octanoic acid (8-BOA) is a selective and potent mechanism-based inactivator (MBI) of CYP4Z1 that can effectively inhibit this enzyme's production of 14,15-epoxyeicosatrienoic acid (14,15-EET) (Kowalski *et al.* 2020), a pro-angiogenic and pro-metastatic metabolite of arachidonic acid (McDonald *et al.* 2017). While cell culture studies can be utilized to interrogate the role of CYP4Z1 in breast cancer, the lack of interaction with a tumour microenvironment limits the predictive power of these experiments (Murayama and Gotoh 2019). Therefore, to further the validation of CYP4Z1 as a drug target in breast cancer, a more complex cellular milieu, with its attendant heterogeneity of signalling ligands, is desirable for inhibitor testing.

The utility of the rat in pre-clinical rodent models of human disease has become increasingly clear due to the many physiological similarities between the species that are absent when using mice. The benefits are especially pronounced for breast cancer studies, as xenografted tumours in rats better parallel those in humans in regard to oestrogen dependency, hormone therapy sensitivity, development, ductal origin, and simulation of phenotypic heterogeneity (Smits *et al.* 2007, Iannaccone and Jacob 2009, Mollard *et al.* 2011). Additionally, recent advances in the generation of immunodeficient rats has furthered the use of this species in varied transplant settings, such as cell- or patient-derived xenograft

CONTACT John P. Kowalski john.kowalski@pfizer.com University of Washington Seattle Campus, Seattle 98195-0005, WA, USA
Supplemental data for this article can be accessed here.

(CDX/PDX) models of tumour growth (Noto *et al.* 2018, He *et al.* 2019).

Therefore, the aim of this pilot-scale study was to assess the *in vivo* characteristics of 8-BOA in the rat to facilitate the design of future CDX/PDX model breast cancer studies with this inhibitor. Specifically, our goals were to assess plasma exposure for feasibility of target enzyme inactivation, characterize circulating metabolites, and interrogate off-target CYP inactivation for 8-BOA.

Materials and methods

Reagents

The stocks of 8-BOA and 6-[(1H-1,2,3-benzotriazol-1-yl)amino]hexanoic acid (6-BHA) used for all experiments were synthesized for our previous study (Kowalski *et al.* 2020). Benzotriazole-d_4 was purchased from CDN Isotopes (Pointe-Claire, Canada) and was used for inhouse synthesis of the deuterated internal standard (see below). Pooled rat (male Sprague Dawley) plasma and urine used as the matrix for protein binding and standards for 8-BOA quantification was purchased from BioIVT (Westbury, NY). Pooled rat (male Sprague Dawley) liver and kidney microsomes (RLM, RKM), derived from control and treated group rats for *ex vivo* experiments, were generated according to standard procedures for subcellular fractionation (Sadeque *et al.* 1992), and quantified *via* BCA assay (Thermo Fisher Scientific, Waltham, MA) according to the manufacturer's protocol. RLM and RKM used for *in vitro* experiments were purchased from Sekisui Xenotech (Kansas City, KS). Chloroform-d was purchased from Cambridge Isotope Laboratories, Inc (Andover, MA), reduced β-nicotinamide adenine dinucleotide phosphate (NADPH) was purchased from OYC Americas (Vista, CA), and formulation reagents (DMSO, PBS, and Solutol) were provided by Alliance Pharma. All solvents (Optima grade) were purchased from Thermo Fisher Scientific, and all other chemicals were purchased Sigma-Aldrich (St. Louis, MO).

Internal standard synthesis

8-{[(4,5,6,7-$^2H_4$)-1H-1,2,3-benzotriazol-1-yl]amino}octanoic acid (8-BOA-d_4) was synthesized using a modified protocol from our previous study and has been summarized in Figure S1. The additional step, amination of benzotriazole-d_4, was performed analogous to a previously reported method (Campbell and Rees 1969). Accurate mass was determined *via* UPLC-MS on a Waters Acquity UPLC (Milford, MA) coupled to an AB Sciex TripleTOF 5600 mass spectrometer (Framingham, MA). ^{1}H NMR spectra was recorded at 25 °C in deuterated chloroform on a 499.73 MHz Agilent DD2 (Santa Clara, CA) spectrometer. Purity as determined by ^{1}H NMR spectroscopy was $\geq$95%. ^{1}H NMR (500 MHz, Chloroform-d) δ ppm 3.42 (t, J = 7.09 Hz, 2 H), 2.35 (t, J = 7.34 Hz, 2 H), 1.59–1.69 (m, 2 H), 1.54 (quin, J = 7.21 Hz, 2 H), 1.40–1.49 (m, 2 H), 1.31–1.38 (m, 4 H). HRMS (ESI$^+$) *m/z* $[M+H]^+$ calculated ($C_{14}H_{17}D_4N_4O_2$) 281.1910, observed 281.1909, δ ppm 0.4.The ^{1}H NMR spectrum for 8-BOA-d_4 has been provided in Figure S2(A) and the ^{1}H NMR spectrum for 8-BOA has been provided in Figure S2(B) for a comparison (reproduced from Kowalski *et al.* 2020 with the authors' permission).

Depletion assays

To assess microsomal stability, the depletion of 8-BOA (and assay controls) was assessed after extended incubation in fortified microsomes. Reactions were set up on ice in triplicate and contained 0.5 mg/mL of either RLM or RKM, in 100 mM potassium phosphate (KPi), pH 7.4, and 3.2 mM $MgCl_2$, in a final volume of 0.5 mL. 8-BOA was added to both RLM and RKM reactions, while 7-hydroxy coumarin and midazolam were added only to RLM reactions; all substrates were diluted 400-fold v/v from DMSO stocks, to achieve final concentrations of 1 μM (reactions contained 0.25% v/v DMSO). After a 5 min equilibration at 37 °C, the reactions were initiated by the addition of a mixture of NADPH, uridine 5′-diphosphoglucuronic acid (UDPGA), and alamethicin, a commonly added pore-forming reagent for *in vitro* investigation of uridine 5′-diphospho-glucuronosyltransferase (UGT)-mediated metabolism, to achieve final concentrations of 1.5 mM, 5 mM, and 10 μg/mL, respectively. Aliquots (50 μL) were removed at times 0, 5, 15, 30, 60, and 90 min and added to tubes containing identical volumes of ice-cold acetonitrile containing 0.5 μM of the internal standard 8-BOA-d_4 (for 8-BOA stability studies) or 7-hydroxy coumarin-d_3 (for 7-hydroxy coumarin and midazolam stability studies) to quench the reactions. All quenched reactions were stored at −20 °C until the end of the experiment. The samples were centrifuged for 10 min at 10,000 x g and 4 °C, and then the supernatants were transferred to new tubes. For quantitation, calibration curves were prepared by separately spiking unlabelled standards for each test compound into an identical microsomal matrix spanning concentrations of 30 nM–3 μM, in half-log dilutions, and underwent sample workup identical to that described above. Aliquots for all samples (5 μL) were then analysed according to the *General LC-MS/MS method for the quantitation of 8-BOA, 6BHA, and assay controls* described below.

General LC-MS/MS method for the quantitation of 8-BOA, 6-BHA and assay controls

Aliquots were analysed by UPLC-MS/MS on a Waters Acquity UPLC connected to a Waters Xevo TQ-S instrument in ESI$^-$ mode, with the following settings: capillary 2.0 kV, source offset 60.0 V, source temperature 150 °C, desolvation temperature 350 °C, cone gas flow 150 L/hr, desolvation gas flow 800 L/hr, collision gas flow 0.15 mL/min, cone voltage 30 V, and collision energy 15 eV. Chromatographic separation of analytes was achieved using a Waters BEH C_{18} column (2.1 × 50 mm, 1.7 μm), starting with 90% mobile phase A (0.1% formic acid in water) and 10% mobile phase B (0.1% formic acid in acetonitrile) at a flow rate of 0.3 mL/min. After a 1 min hold, B was increased linearly from 10 to 95% between 1 and 3 min and held at 95% between 3.5 and 5.5 min; the total run time was 7 min following a 1.5 min

period for equilibration. The analytes and isotope-labeled internal standards were detected by multiple reaction monitoring (MRM) in electrospray negative mode (ESI^-) with the following transitions and retention times: 8-BOA *m/z* 275.15 > 154, 8-BOA-d_4 279.16 > 154 (2.9 min), warfarin 307 > 161, warfarin-d_5 312 > 161 (3.2 min), and 6-BHA 247 > 118 (2.7 min). The following were detected by MRM in ESI^+ mode: 7-hydroxy coumarin *m/z* 163 > 119, 7-hydroxy coumarin-d_3 166 > 122 (2.4 min), and midazolam 327 > 292 (2.5 min). Analysis of the mass spectra was performed with Waters MassLynx V4.1.

Plasma protein binding

In vitro analysis of plasma protein binding (PPB) was performed for 8-BOA, 6-BHA, and Warfarin as an assay control. Compounds were spiked separately into pooled male Sprague Dawley rat plasma to achieve final concentrations of 3 μM. A dialysis method was followed using rapid equilibrium dialysis devices according to the manufacturer's protocol (ThermoFisher Scientific). After the incubation period, ice-cold acetonitrile, containing the internal standard 8-BOA-d_4 (for both 8-BOA and 6-BHA samples), or Warfarin-d_5, at 0.5 μM and 0.1% formic acid was added at a 3:1 ratio. The samples were centrifuged for 10 min at 10,000 x g and 4 °C, and then the supernatants were transferred to new tubes. Aliquots for all samples (5 μL) were then analysed according to the *General LC-MS/MS method for the quantitation of 8-BOA, 6BHA, and assay controls*.

Determination of CYP content

In vitro inactivation

Inactivation reactions were set up on ice and contained RLM (Sekisui Xenotech) at 1 mg/mL in 100 mM KPi, pH 7.4 and 3.2 mM $MgCl_2$, in a final volume of 1.2 mL. 8-BOA was diluted 400-fold v/v from DSMO stocks to achieve final concentrations of 100 and 500 μM, or an equal volume of DMSO was added (reactions contained 0.25% v/v DMSO). After a 5 min period for equilibration at 37 °C, NADPH was added (1 mM final concentration) to all conditions to initiate the reactions. Following a 30 min incubation, 0.55 mL aliquots were removed from each condition and immediately placed into either a sample or reference cuvette. CYP content was then measured with an Olis Aminco DW-2 spectrophotometer (Bogart, GA) following the standard procedure for carbon monoxide (CO) binding difference spectra (Guengerich *et al.* 2009). Note: reactions were performed at separate times to ensure incubation time consistency between conditions.

Ex vivo CYP content

Mixtures were set up on ice in duplicate and contained either pooled RLM or RKM, that were derived from treated or control group rats, at concentrations of 2 mg/mL in 100 mM KPi, pH 7.4, with 0.5% sodium cholate w/v, in a final volume of 1.2 mL. 0.55 mL aliquots for each condition were split between sample and reference cuvettes and CYP content was measured as described above.

Animal studies

Animal procedures were performed in full compliance with all applicable regulations by Alliance Pharma (Malvern, PA). Following a two day facility acclimation period, three male Sprague Dawley rats, weighing between 0.307–0.316 kg, received intravenous (IV) bolus administration of 8-BOA (4 mg/mL in PBS, 67%; Solutol, 30%; DMSO, 3%) at 10 mg/kg and a dose volume of 2.5 mL/kg. A control group of three rats, weighing between 0.303–0.320 kg, received the same formulation as above, minus 8-BOA. The study proceeded for 24 hours and serial blood collections (tail bleeds) were taken at pre-dose, 5, 15, 30 min, 1, 2, 4, 8, and 24 hr, and plasma was separated. After euthanasia, necropsies were performed and liver and kidney were collected from each animal, and urine was collected from the bladders. Samples were then shipped on dry ice overnight for inhouse bioanalysis. Standard clinical chemistries were performed by Phoenix Lab (Mukilteo, WA) on plasma from both control and treated groups for pre-dose and 24-hour timepoints.

Determination of 8-BOA and 6-BHA plasma concentrations and pharmacokinetic analysis

Plasma samples were thawed on ice and 20 μL aliquots were transferred to new tubes. To these, 60 μL of ice-cold acetonitrile, containing 5 μM 8-BOA-d_4 and 0.1% formic acid, was added. The samples were centrifuged for 10 min at 10,000 x g and 4 °C, and then the supernatants were transferred to new tubes. A calibration curve was prepared for quantification; 8-BOA or 6-BHA was spiked into pooled male Sprague Dawley rat plasma diluted 200-fold v/v from DMSO stocks to achieve concentrations ranging from 1 nM–1 mM, in half-log dilutions (DMSO control was also prepared). The standards were subjected to the same sample workup as described above and aliquots for all samples (5 μL) were then analysed according to the *General LC-MS/MS method for the quantitation of 8-BOA, 6BHA, and assay controls*.

The quantitation data for both 6-BHA and 8-BOA were subjected to non-compartmental analysis (NCA) using Certara WinNonlin (Princeton, NJ) with standard settings. Furthermore, after plotting the time – concentration profile, the 8-BOA data was also fit to the standard 2-compartment model using Graphpad Prism 7.00 (San Diego, CA) according to the following equation:

$$C = Ae^{-\alpha t} + Be^{-\beta t} \quad (1)$$

Pharmacokinetic parameters were subsequently calculated using the resultant hybrid constants (for comparison to NCA) and this equation was used to calculate plasma 8-BOA concentrations for the CYP4Z1 inactivation simulations (described later).

Metabolite identification

Sample preparation

Equal volumes of remaining plasma were separately pooled from the time points spanning 5-min to 24-hr for treated and control group rats. A 6-fold volume of ice-cold acetonitrile was added, the samples vortexed briefly, centrifuged for 10 min at 10,000 x g and 4 °C, and then the supernatants were transferred to new tubes. The samples were dried under a constant stream of N_2 at room temperature, resuspended in 150 μL of a 70/30 mixture of water/acetonitrile, and then stored at 4 °C until use.

Equal volumes of urine from the bladder collections at the 24-hr time point for the control group as well as for the 8-BOA treated rats were combined and the internal standard 8-BOA-d_4 was spiked in to achieve a final concentration of 100 nM (to enable quantification of any remaining 8-BOA parent). To create a callibration curve, pooled male Sprague Dawley rat urine was spiked with 8-BOA diluted 200-fold v/v from DMSO stocks to achieve final concentrations from 1–1000 nM, in half-dilutions, and 8-BOA-d_4 was added to achieve a final concentration of 100 nM. The pH was adjusted to ~2 with acetic acid for all urine samples and they were subsequently extracted three times with a 50/50 mixture of diethyl ether/ethyl acetate. The combined organic fractions were dried under a constant stream of N_2 at room temperature, resuspended in 150 μL of a 70/30 mixture of water/acetonitrile, and then stored at 4 °C until use. A portion was assayed for 8-BOA concentration according to the *General LC-MS/MS method for the quantitation of 8-BOA, 6BHA, and assay controls.*

Qualitative LC-MS/MS profiling for 8-BOA rat metabolites

Aliquots (30 μL) were analysed by UPLC-MS/MS on a Waters Acquity UPLC connected to an AB Sciex TripleTOF 5600 mass spectrometer in both ESI ± modes (separately) with parent and product ions acquired concurrently in the same period using settings for experiment 1 and 2, respectively. For experiment 1, TOF MS scanning was restricted to a 50–1000 Da range with a cycle time of 0.55 sec and an accumulation time of 0.1 sec. Information dependent acquisition (IDA) used switch criteria settings that required ions to be >100 *m/z*, exceed 150 cps, and to exclude former target ions for 1 second. The nominal mass of 8-BOA was set to 276 Da, a 700 Da formula width was used, and a mass defect of 158.6261 mDa was applied; mass tolerance was 50 mDa. Settings for DP, CE, and XA1 were 100, 5, and 136.62, respectively. For experiment 2, TOF MS/MS scanning was again restricted to a 50–1000 Da range with an accumulation time of 0.1 sec. For this product ion acquisition, settings for DP, CE, CES, IRD, IRW, and XA1 were 100, 35, 20, 67, 25, and 70.16, respectively. For both experiment 1 and 2, settings for GS1, GS2, CUR, TEM, and ISVF were 60, 60, 35, 600, and 4500, respectively.

Chromatographic separation of analytes was achieved using a Waters SunFire C_{18} column (2.1 × 150 mm, 3.5 μm), starting with 100% mobile phase A (0.1% formic acid in water) and 0% mobile phase B (0.1% formic acid in acetonitrile) at a flow rate of 0.3 mL/min. After a 1 min hold, B was increased linearly from 0 to 100% between 1 and 14 min and held at 100% between 14 and 15.1 min; the total run time was 20 min following a 4.9 min period for equilibration. Analysis of the mass spectra was performed with SCIEX Metabolite Pilot V2.0 with the settings as described below.

Metabolite Pilot settings

8-BOA and 6-BHA were each run as parent compounds (as 6-BHA was identified later as a major metabolite that downstream biotransformation processes could conceivably occur to), therefore reference MS/MS spectra for both was provided. Control group samples for both urine and plasma matrices were run in conjunction with the treated group and acted as the background filtering control for metabolite peaks. The processing parameters for Metabolite Pilot in both ESI ± modes consisted of the following TOF MS settings: predicted metabolites, generic peak finding, application of mass defect filter, and isotope pattern. The TOF MS/MS settings consisted of the following: find at least 2 characteristic product ions, find at least 1 characteristic neutral loss, and consider internal neutral losses. The biotransformation set contained 100 phase I/II and amino acid conjugation pathways. MS *m/z* tolerance was set to 20 ppm and the minimum MS peak intensity was set to 200 CPS; MS/MS *m/z* tolerance was set to 10 mDa and the minimum MS/MS peak intensity was set to 100 cps. In addition to identifying protonated/deprotonated metabolites, other common adducts were also searched for. Results were manually filtered and metabolites were excluded that either a) completely lacked MS/MS spectra (and weren't identified in the other ESI mode), b) showed a < 10-fold difference in signal intensity between control and sample, c) were readily interpreted as in-source fragmentation (unless they were notable and hence were included), or d) displayed peak chromatography consistent with a slight offset to a control peak and therefore was artifactually identified as a metabolite by the program.

CYP activity assays

Reaction set-up

For CYP activity comparisons between the pooled RLM derived from treated and control group rats, the probe substrates and the biotransformations that were monitored (all done separately) were as follows: CYP1A/-2C phenacetin *O*-deethylation, CYP2C/-2D dextromethorphan *O*-demethylation, and CYP3A/-CYP2C midazolam 1′-hydroxylation. Reactions were set up on ice in triplicate and contained microsomes at 0.25 mg/mL protein in 100 mM KPi pH 7.4, with 3.2 mM $MgCl_2$, in a final volume of 200 μL. The above listed probe substrates were each added independently from DMSO stocks, diluted 400-fold v/v, to the reactions to achieve final concentrations of 10 μM (reactions contained 0.25% v/v DMSO). After a 5 min period at 37 °C for equilibration, the reactions were started by the addition of NADPH at a final concentration 1 mM. The reactions were quenched after 20 min with an equal volume of ice-cold acetonitrile

containing a mix of all deuterated internal standards at a concentration of 200 nM each. The samples were centrifuged for 10 min at 10,000 x g and 4 °C, and then the supernatants were transferred to new tubes. For quantitation, metabolite standards were spiked all together into an identical matrix to attain concentrations spanning 0.001–1 μM, in half-log dilutions, and underwent sample workup identical to what is described above.

LC-MS/MS method for quantification of probe substrate metabolites

Aliquots (5 μL) were analysed by UPLC-MS/MS on a Waters Acquity UPLC connected to a Waters Xevo TQ-S instrument in ESI^+ mode, with the following settings: capillary 2.9 kV, source offset 60.0 V, source temperature 150 °C, desolvation temperature 350 °C, cone gas flow 150 L/hr, desolvation gas flow 800 L/hr, collision gas flow 0.15 mL/min, cone voltage 40 V, and collision energies of 20 eV for acetaminophen and 30 eV for the other analytes. Chromatographic separation utilized a Waters HSS T3 column (2.1 × 100 mm, 1.8 μm), starting with 95% mobile phase A (0.1% formic acid in water) and 5% mobile phase B (0.1% formic acid in acetonitrile) at a flow rate of 0.3 mL/min. After a 1 min hold, B was increased linearly from 5 to 60% between 1 and 7 min, immediately increased to 95%, and then held at 95% between 7 and 8.5 min; the total run time was 11 min following a 2.5 min period for equilibration. The metabolites and isotope-labeled internal standards were detected by MRM with the following transitions and retention times: acetaminophen *m/z* 152 > 110, acetaminophen-d_3 155 > 111 (3.3 min), dextrorphan 258 > 157, dextrorphan-d_3 261 > 157 (4.5 min), 1-hydroxymidazolam 342 > 203, and 1-hydroxymidazolam-d_4 346 > 203 (5.4 min). Analysis of the mass spectra was performed with Waters MassLynx V4.1 software.

Kinetics of CYP4Z1 inactivation from 6-BHA

Inhibition and probe substrate reactions were setup and run analogous to the method in our previous study and LC-MS/MS quantification was also similarly run (Kowalski *et al.* 2020). Briefly, in reactions containing 5 pmol CYP4Z1, 6-BHA was diluted 400-fold v/v from DMSO stocks to achieve final concentrations of 0, 6, 10, 20, 40, 60, 80, and 120 μM (reactions contained 0.25% v/v DMSO), and aliquots of the inhibition reactions were taken at times of 0, 5, 10, and 15 min for the residual activity reactions, using the probe substrate luciferin-benzyl ether (Luc-BE).

CYP inactivation simulations

The extrapolation of 8-BOA plasma concentrations to inactivation of the target CYP4Z1, in a theoretical rat xenograft, was performed using the 2-compartment model Equation (1) outlined above to calculate drug concentrations ([drug]), and then using the following equations:

$$[drug]_{free} = f_u \times [drug] \tag{2}$$

$$\lambda = ([drug]_{free} \times k_{inact})/([drug]_{free} + K_I) \tag{3}$$

$$ActiveCYP4Z1enzyme(\%) = \left(e^{-(\lambda + k_{deg}) \times \Delta t} + (k_{deg} \times \Delta t)\right) \times 100 \tag{4}$$

The simulation was performed in Excel with the following parameters:

$$f_u = 0.02$$

$$k_{inact} = 0.15 min^{-1}$$

$$K_I = 2.2 \mu M \left(K_I = 0.61 \frac{\mu g}{mL}\right)$$

$$k_{deg} = 0.00048 min^{-1} \left(t_{1/2,CYP} = 1 day\right)$$

$$k_{deg} = 0.00024 min^{-1} \left(t_{1/2,CYP} = 2 days\right)$$

$$k_{deg} = 0.00012 min^{-1} \left(t_{1/2,CYP} = 4 days\right)$$

$$\Delta t = 15 min.$$

Values for $[drug]_{free}$ and λ were determined for each time-point of the time-step. Starting from time zero (100% active CYP4Z1), all subsequent values calculated for active CYP4Z1 enzyme were performed on the previously calculated fraction (and converted to percent) such that inactivation was iterative with time. Plasma $drug_{free}$ concentrations were assumed to equal intratumoral concentrations, the tumour was assumed to be in the central compartment, and the microsomal protein binding of 8-BOA for the *in vitro* conditions used to calculate k_{inact} and K_I in CYP4Z1 membranes was assumed to be minimal. Although not determined experimentally, if microsomal binding of 8-BOA to membranes were substantial, this would result in a lowered effective K_I and increased potency of inactivation in this model.

Results

Metabolic stability

In order to evaluate microsomal stability and the summative (potentially sequential) contributions of CYP- and uridine 5′-diphospho-glucuronosyltransferase (UGT)- mediated metabolism to clearance, 8-BOA at an initial concentration of 1 μM was incubated for an extended period with RLM or RKM that had been fortified with NADPH and UDPGA. After 90 min, 8-BOA concentrations were reduced by ~6 and ~4% for RLM and RKM, respectively (Figure 1(A)). Minimal depletion was also evident when 3 μM of 8-BOA was used (data not shown). Although calculation of an *in vitro* microsomal $t_{1/2}$ for 8-BOA was not practical due to the negligible decline and margin of error for measurements, we estimate these values to be >12 hr. In control RLM studies, midazolam and 7-hydroxy coumarin depletion both displayed *in vitro* $t_{1/2}$ values of <5 min (data not shown).

Off-target CYP inactivation

To assess degree of off-target microsomal CYP inactivation caused by 8-BOA, carbon-monoxide (CO)-binding spectra were recorded for NADPH-fortified RLM after incubation with 8-BOA or DMSO vehicle (Figure 1(B)). After 30-minute incubations the CYP contents were 0.62, 0.57, and 0.34 nmol/mg

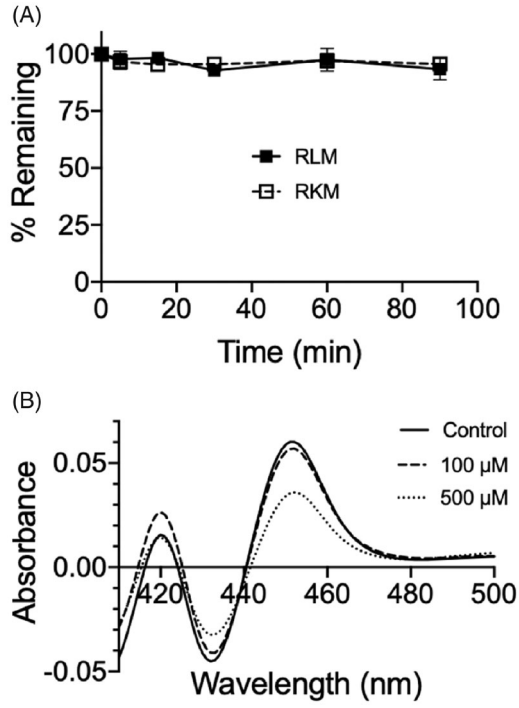

Figure 1. *In vitro* assessment of metabolic stability and off-target CYP inactivation. 8-BOA (1 μM) was incubated with pooled RLM or RKM (Xenotech) in the presence of NADPH (1.5 mM), UDPGA (5 mM), and alamethicin (10 μg/mL). Minimal depletion of 8-BOA was observed in either microsomal system over the course of 90 minutes. Shown is the average and standard deviation from three replicates (A). Pooled RLM was incubated in the presence of NADPH for 30 minutes with either DMSO (control) or 8-BOA, and standard CO-difference spectra was recorded for each sample. Absorbance at 450 nm decreased with increasing concentrations of 8-BOA, resulting in a ~7 and ~45% reduction of total CYP content at 100 and 500 μM, respectively.

protein for the DMSO control, 100, and 500 μM of 8-BOA, respectively. This equates to dose-dependent losses of 7-45% in liver microsomal CYP content.

Plasma protein binding (PPB)

As determined by rapid equilibrium dialysis with LC-MS/MS quantitation, 8-BOA and 6-BHA (3 μM) were bound 98 ± 0.20 and 75 ± 4.0%, respectively, to rat plasma proteins. Warfarin, used as an assay control, was bound 99 ± 0.10%, as expected. A recognized limitation is that only single concentrations of ligands were tested, as such, linearity was not assessed.

Pharmacokinetics of 8-BOA and 6-BHA

The time-concentration profile of 8-BOA in plasma after IV bolus administration at 10 mg/kg is shown in Figure 2. Inter-animal variability was relatively low, and the profile exhibited a multi-exponential pattern, indicative of both distribution and elimination phases being present. The pharmacokinetic constants resulting from non-compartmental analysis (NCA) are summarized in Table 1. Prolonged, albeit low, exposure to 8-BOA was observed, characterized by an extended $t_{1/2}$ and low *CL*. The standard whole body 2-compartmental model was also fit to the data, which yielded the following hybrid values: A = 43.45, α = 3.32, B = 0.068, β = 0.12; this

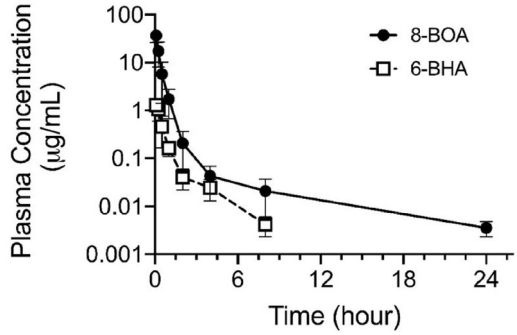

Figure 2. Plasma time-concentration profile for 8-BOA, administered *via* IV bolus at 10 mg/kg, and the metabolite 6-BHA, in male Sprague Dawley rats. Non-compartmental analysis was utilized to calculate pharmacokinetic parameters. Shown is the average ± SD ($n = 3$).

Table 1. Pharmacokinetic parameters for 8-BOA and 6-BHA.

Parameter	8-BOA	6-BHA
T_{max} (hr)	–	0.14 ± 0.10
C_{max} (μg/mL // μM)	37 ± 10 // 130 ± 36	1.5 ± 0.14 // 6.1 ± 0.10
C_0 (μg/mL // μM)	55 ± 6.5 // 200 ± 24	–
$t_{1/2,\ elim.}$ (hr)	6.1 ± 1.0	1.8 ± 0.20[a]
$AUC_{0\rightarrow\infty}$ (hr*μg/mL)	14 ± 5.8	0.84 ± 0.20
CL (mL/min/kg)	14 ± 7.3	–
V_z (L/kg)	7.9 ± 4.8	–
V_{ss} (L/kg)	0.59 ± 0.50	–

Shown are the averages ± SD ($n = 3$)
[a]Terminal phase likely not fully characterized

enabled the calculation of 8-BOA concentrations for the time-steps required for simulating CYP4Z1 inactivation. To assess goodness of fit, a residual plot was analysed which showed a random pattern, indicating that the application of the 2-compartment model to the 8-BOA data was acceptable (data not shown).

The time-concentration profile of the metabolite 6-BHA in plasma is also depicted in Figure 2. NCA yielded values for T_{max}, C_{max}, $t_{1/2}$, and *AUC*, which are summarized in Table 1.

Metabolite identification

Plasma profiling

LC-MS/MS analysis was performed in both ESI^+ and ESI^- mode to ensure the best coverage of analytes, since ESI^- would likely be required to detect some acid-containing metabolites. Given the complexity of the matrices involved, this ensured that mass-defect filtering with information-dependent acquisition (IDA) would have the most opportunities to trigger MS/MS fragmentation required for metabolite identification.

A complex profile of 25 total metabolites were detected by LC-MS/MS in the plasma of rats following IV administration of 8-BOA. The extracted ion chromatograms (XICs) for both ESI^+ and ESI^- modes used for metabolite identification are shown in Figure 3. While **M3 – M10, M13, M15,** and **M16** were detected in both modes, **M1, M2, M11, M12** and **M14** were detected only in ESI^+, and **M17 – M25** were detected only in ESI^-. Given that the plasma was pooled from timepoints spanning 5 min–24 hr, in order to increase

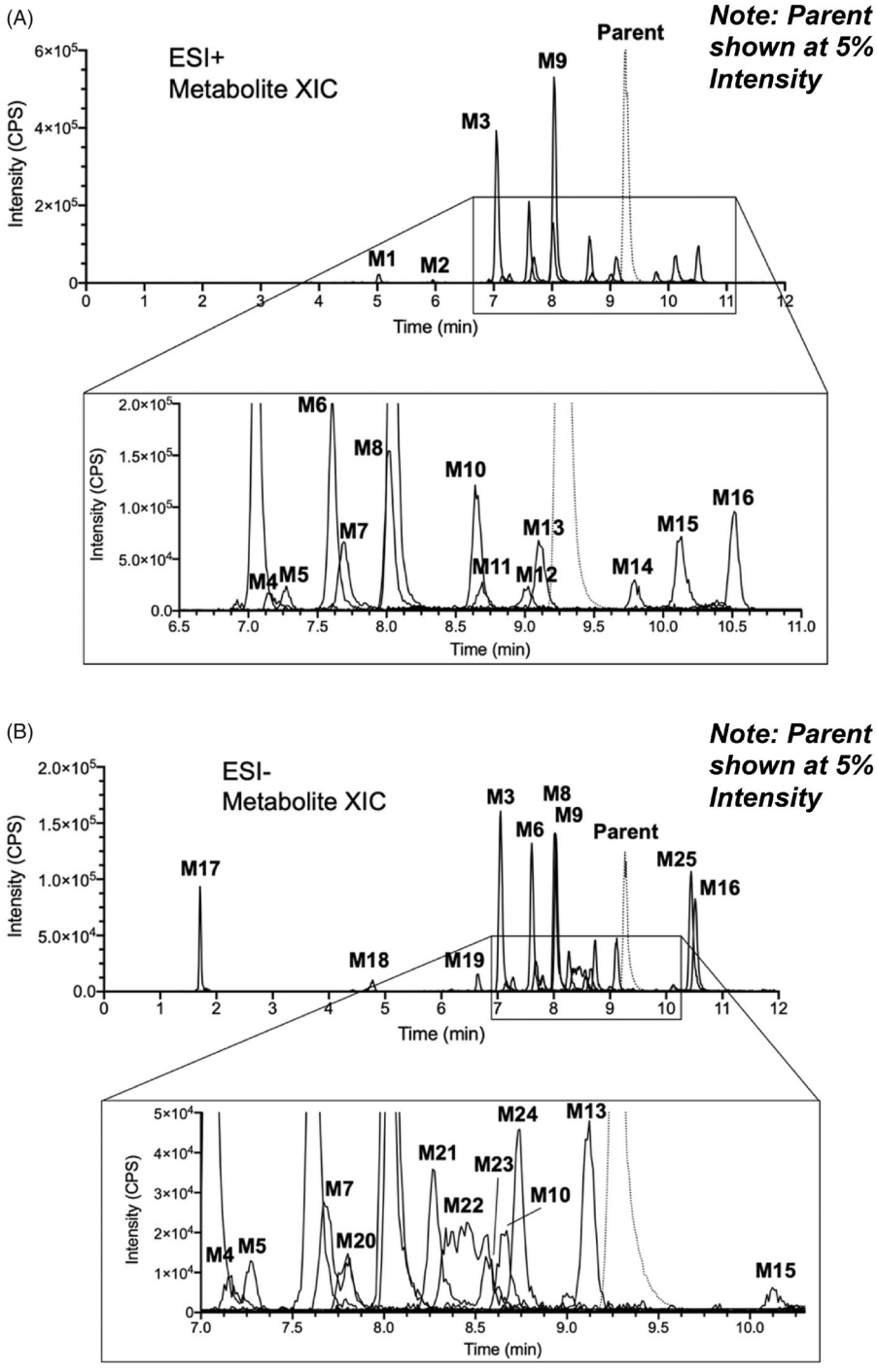

Figure 3. Metabolite identification in pooled rat plasma (5-min to 24-hr) *via* LC-MS/MS analysis. Overlaid extracted ion chromatograms (XIC) for detected metabolites in ESI^+ mode. The metabolites **M3** (loss of $(CH_2)_4$), **M9** (loss of $(CH_2)_2$), **M6** (hydroxylated), and **M8** (hydroxylated), displayed the largest peak areas (**A**). Overlaid XIC for detected metabolites in ESI^- mode; metabolites with the largest peak areas matched that which were observed in ESI^+ mode (**B**). **M1, M2, M11, M12** and **M14** were detected only in ESI^+, **M17 – M25** were detected only in ESI^-, and **M3 – M10, M13, M15, M16** were detected in both modes. The **Parent** (8-BOA, dotted peak) eluted at 9.3 min and has been plotted at 5% of intensity in both ESI^+ and ESI^- modes for visual comparison; numerous metabolites show intensities approximately $\leq$5% that of the **Parent**.

metabolite MS counts, the **Parent** 8-BOA constituted a dominant signal. Therefore, the chromatograms showing metabolites in both modes have the **Parent** peak plotted at 5% of the detected intensity for ease of viewing. In ESI^+ mode, **M9, M3, M6,** and **M8** were the major metabolites by peak area, and accounted for 67% of the total profile, with **M9** and **M3** themselves accounting for 28 and 20%, respectively. These same four metabolites accounted for 48% of the total profile in ESI^- mode.

ESI^+ plasma metabolite assignments

All metabolites were observed as the protonated ion $[M+H]^+$, except **M1** as $[M]^+$, and these were absent from

Table 2. Plasma metabolites identified in ESI+ mode.

Peak ID	Biotransformation	Formula	*m/z*	ppm	R.T. (min)	Peak Area
Parent	N/A (8-BOA) [M + H]+	$C_{14}H_{20}N_4O_2$	277.1662	1.2	9.26	7.83E + 07
M1	-$(CH_2)_4$+Carnitine [M]+	$C_{17}H_{26}N_5O_4$	364.198	0.2	5.04	9.59E + 04
M2	-$C_8H_{14}O_2$ [M + H]+	$C_6H_6N_4$	135.0667	1.4	5.96	1.80E + 04
M3	-$(CH_2)_4$ [M + H]+	$C_{10}H_{12}N_4O_2$	221.1034	0.3	7.04	1.73E + 06
M4	Oxidation [M + H]+	$C_{14}H_{20}N_4O_3$	293.1607	−0.3	7.14	5.79E + 04
M5	Oxidation [M + H]+	$C_{14}H_{20}N_4O_3$	293.1609	0.4	7.27	9.44E + 04
M6	Oxidation [M + H]+	$C_{14}H_{20}N_4O_3$	293.1609	0.4	7.61	8.74E + 05
M7	Ketone Formation [M + H]+	$C_{14}H_{18}N_4O_3$	291.1453	0.5	7.69	3.68E + 05
M8	Oxidation [M + H]+	$C_{14}H_{20}N_4O_3$	293.1607	−0.3	8.01	7.53E + 05
M9	-$(CH_2)_2$ [M + H]+	$C_{12}H_{16}N_4O_2$	249.1347	0.4	8.03	2.44E + 06
M10	-$(CH_2)_2$+Methylation [M + H]+	$C_{13}H_{18}N_4O_2$	263.1502	−0.2	8.64	5.69E + 05
M11	Desaturation [M + H]+	$C_{14}H_{18}N_4O_2$	275.1505	0.8	8.69	1.36E + 05
M12	Desaturation [M + H]+	$C_{14}H_{18}N_4O_2$	275.1506	1.4	9.02	1.40E + 05
M13	Ketone + Methylation [M + H]+	$C_{15}H_{20}N_4O_3$	305.1608	−0.1	9.10	3.51E + 05
M14	Methylation [M + H]+	$C_{15}H_{22}N_4O_2$	291.1813	0.3	9.79	1.49E + 05
M15	Desaturation [M + H]+	$C_{14}H_{18}N_4O_2$	275.1503	0.1	10.13	4.12E + 05
M16	2x Methylation [M + H]+	$C_{16}H_{24}N_4O_2$	305.1976	1.3	10.51	4.59E + 05

pooled plasma derived from the control group (Table 2). LC-MS/MS analysis of the reference standard for the **Parent** 8-BOA (Figure S3**)** was identical to that observed in plasma and provided diagnostic fragments, e.g., *m/z* 135, 119, and 90, which aided in metabolite assignments. Characteristic dehydration of the carboxylic acid (minus 18 Da) and dehydration plus loss of N_2 (minus 46 Da) were also commonly observed. For ease of viewing, the annotated structure fragment ions are listed without defect values. These are shown in the MS/MS spectra where differential defects from equivalent nominal masses can be discerned between structures.

The largest metabolite by peak area, **M9** (*m/z* 249.13 $[M+H]^+$), was assigned as having the formula $C_{12}H_{16}N_4O_2$ that corresponded to the **Parent** 8-BOA undergoing one round of β-oxidation (loss of two methylene units). **M9** displayed ions *m/z* 231, corresponding to dehydration, and *m/z* 203, corresponding to dehydration plus loss of N_2 (Figure 4(A)). The MS/MS and retention time of **M9** was identical to that of the reference standard for the chain-shortened analog 6-[(1H-1,2,3-benzotriazol-1-yl)amino]hexanoic acid (6-BHA, Figure S3), thus confirming the structure for this major metabolite.

The metabolite with the next greatest peak area, **M3** (*m/z* 221.10 $[M+H]^+$), was assigned the formula $C_{10}H_{12}N_4O_2$, which is consistent with the **Parent** 8-BOA undergoing two rounds of β-oxidation (loss of four methylene units). MS/MS of **M3** identified an ion at *m/z* 175 corresponding to dehydration plus loss of N_2 (Figure 4(B)). Additionally, the retention time of **M3** matched the relative elution progression observed for the **Parent** 8-BOA and the metabolite 6-BHA (**M9**). Therefore, although lacking a reference standard, there is strong evidence for assigning **M3** as 4-[(1H-1,2,3-benzotriazol-1-yl)amino]butanoic acid (4-BBA).

The presence of four mono-hydroxylated metabolites in the profile was indicated by their shorter elution times and gain of 16 Da, relative to the **Parent**, resulting in molecular ions of *m/z* 293.16 $[M+H]^+$, with **M6** and **M8** dominating. The MS/MS spectra for **M6** is shown in Figure 4(C), where sequential dehydration generated fragments of *m/z* 275 and 257, followed by removal of CO to generate *m/z* 231. This fragment ion of *m/z* 231 was unique to **M6** and definitively allows for assignment as the *β*-hydroxy metabolite since cleavage of this bond is diagnostic for such regiospecificity. The concomitant aldehyde that is formed from this fragmentation (oxidation of the former *β*-hydroxyl group) also resulted in the expected ion of *m/z* 233. Similarly, **M8** was assigned as the α-hydroxy metabolite due to the strong signal for the diagnostic ion of *m/z* 247, representing cleavage between the α-hydroxy and carboxylic acid moiety. For **M4** and **M5,** the fragment ions *m/z* 160 and 132 were consistent with oxidation occurring at the γ- through ε-positions of the aliphatic tail, and furthermore, no strong evidence of hydroxylation on the ABT moiety was observed. However, due to the limited MS/MS spectra and lack of reference standards, absolute regiospecificity could not be defined.

The metabolite **M7** (*m/z* 291.14 $[M+H]^+$) exhibited fragmentation consistent with ketone formation at the *β*-carbon, while fragmentation of the desaturation metabolites **M11** and **M12** (*m/z* 275.15 $[M+H]^+$) placed the olefins on the alkyl-acid chain but could not define exact positions. **M15**, another apparent desaturation product from the observed *m/z*, eluted later than the **Parent** and had a matching retention time and accurate mass to an intermediate imine compound (positioned adjacent to ABT) generated during the synthesis of 8-BOA, hence it was assigned as such (data not shown). Various other metabolites were consistent with parent methylations of varying regiospecificity (**M13, M16**), loss of the side chain -$C_8H_{14}O_2$ to generate **M2** (i.e., ABT, also confirmed through a reference standard) and **M1**, the carnitine conjugate of **M3**. All 16 metabolites identified in ESI^+ mode are summarized in Table 2, and the MS/MS spectra that aided in the structural assignments for all metabolites have been provided in the Supporting Information.

ESI^- plasma metabolite assignments

All metabolites were observed as the de-protonated ion $[M-H]^-$ (although other minor adducts were also present) and were absent from pooled plasma derived from the control group (Table 3). In ESI^- mode, the major metabolites **M9, M6,** and **M8** all possessed fragmentation consistent with the previously assigned structures derived from their ESI^+ fragmentation profile, although the ESI^- MS/MS spectra proved less diagnostic in general. While the molecular ion for **M3**

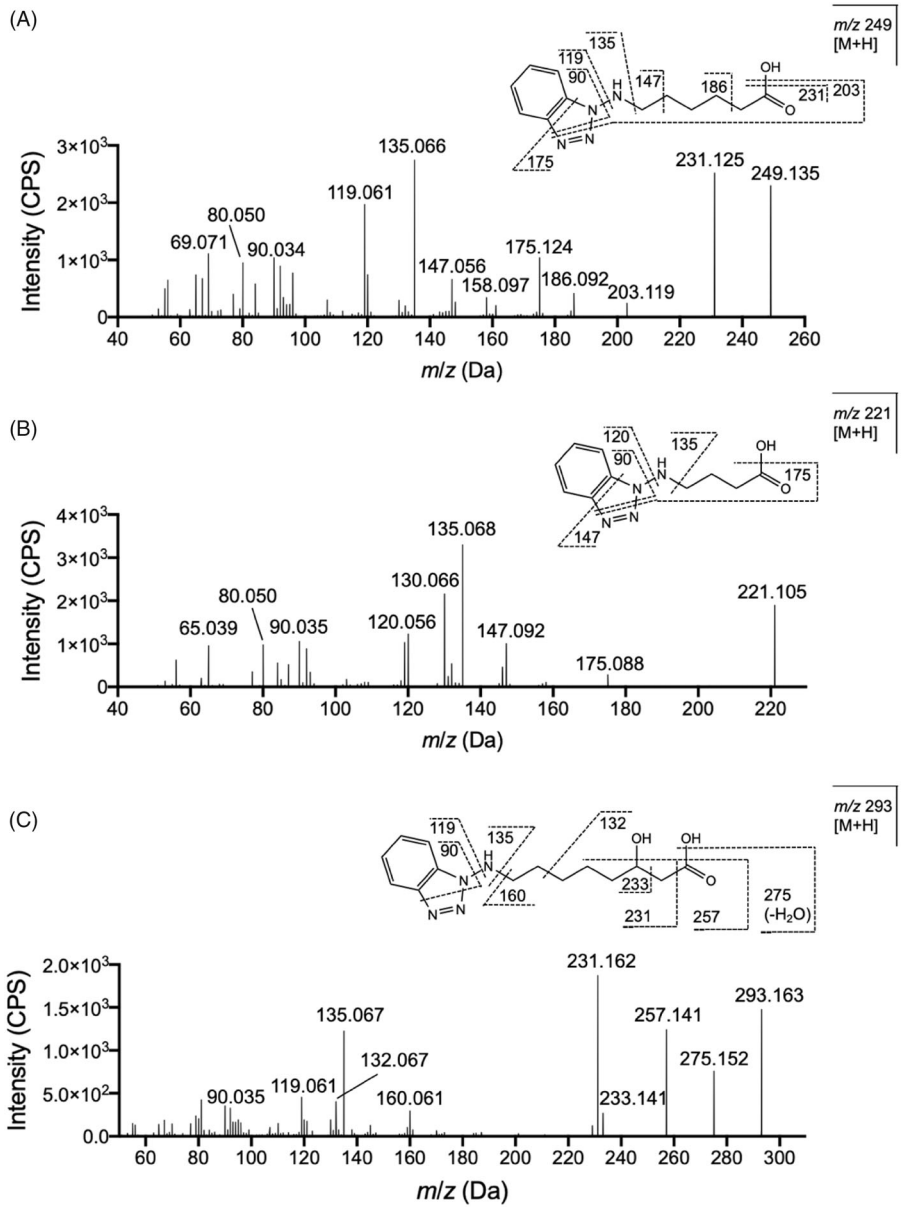

Figure 4. LC-MS/MS analysis, in ESI^+ mode, of the top three metabolites of 8-BOA (by peak area) in pooled rat plasma. **M9**, the metabolite with matching RT and MS/MS as the chain-shortened analog 6-BHA was confirmed as the result of a loss of $(CH_2)_2$ from the **Parent** (A). **M3** shows MS/MS spectra corresponding to a further chain-shortening of 6-BHA, resulting in a loss of $(CH_2)_4$ from the **Parent**, and has been tentatively identified as 4-[(1H-1,2,3-benzotriazol-1-yl)amino]butanoic acid (4-BBA) (B). **M6** (Parent plus 16 Da), shows fragmentation consistent with hydroxylation at the β-carbon of the 8-BOA aliphatic tail (C).

(*m/z* 219.09 $[M-H]^-$) still generated a strong signal, no MS/MS spectral fragments were triggered for this metabolite.

Notably, ESI^- analysis revealed **M20 – M23** as glucuronide conjugates, which in total accounted for ~13% of the total peak area for metabolites observed in this mode (Figure S4(A)**).** **M20** and **M22** had identical mass fragmentation profiles (*m/z* 451.18 $[M-H]^-$) (Figure S4(B)), and were assigned the formula $C_{20}H_{28}N_4O_8$, which is consistent with glucuronidation of the **Parent**. Fragmentation produced the aglycone ion at *m/z* 275, with the corresponding dehydrated glucuronate at *m/z* 175, and the further dehydrated glucuronate minus CO_2 at *m/z* 113. Direct fragmentation evidence for the acyl-glucuronide is provided by the *m/z* 193 ion, which represents the full glucuronate that would be absent for the *N*-glucuronide. Furthermore, the ion at *m/z* 133 confirmed the presence of the ABT moiety. Although only the 1-β anomer is depicted in the annotated scheme, **M20** may in fact be the 1-β anomer while the **M22** cluster likely represents a mix of the 2-, 3- and 4-α/β acyl-glucuronide anomers.

Metabolites **M21** and **M23** also showed similar fragmentation profiles (*m/z* 319.14 $[M-H]^-$) and were assigned the formula $C_{14}H_{24}O_8$, which corresponded to acyl-glucuronide structures of the **Parent** minus the ABT moiety. Fragmentation of **M21** (Figure S4(C)) produced the aglycone ion at *m/z* 143, the expected dehydrated glucuronate at *m/z* 175, and the further dehydrated glucuronate minus CO_2 at *m/z* 113. **M21** and **M23** had nearly overlapping retention times with the aforementioned acyl-glucuronide cluster and therefore may be artifactually generated *via* in-source fragmentation of **M22** or sample work-up.

Table 3. Plasma metabolites identified in ESI- mode.

Peak ID	Biotransformation	Formula	*m/z*	ppm	R.T. (min)	Peak Area
Parent	N/A (8-BOA) [M-H]-	$C_{14}H_{20}N_4O_2$	275.1524	3.7	9.27	2.02E + 07
M17	Unassigned +16.9885	Unassigned	292.1399	N/A	1.71	2.28E + 05
M18	Unassigned +272.9481	Unassigned	548.1005	N/A	4.78	4.02E + 04
M19	-$(CH_2)_2$+Oxidation [M-H]-	$C_{12}H_{16}N_4O_3$	263.1156	2.5	6.66	6.94E + 04
M3	-$(CH_2)_4$ [M-H]-	$C_{10}H_{12}N_4O_2$	219.0896	4.1	7.05	7.51E + 05
M4	Oxidation [M-H]-	$C_{14}H_{20}N_4O_3$	291.1463	0.1	7.17	3.61E + 04
M5	Oxidation [M-H]-	$C_{14}H_{20}N_4O_3$	291.1457	−1.9	7.27	5.45E + 04
M6	Oxidation [M-H]-	$C_{14}H_{20}N_4O_3$	291.1468	1.8	7.61	5.85E + 05
M7	Ketone Formation [M-H]-	$C_{14}H_{18}N_4O_3$	289.1310	1.3	7.67	1.41E + 05
M20	Glucuronidation [M-H]-	$C_{20}H_{28}N_4O_8$	451.1824	−2.3	7.80	8.33E + 04
M8	Oxidation [M-H]-	$C_{14}H_{20}N_4O_3$	291.1465	0.9	8.02	7.20E + 05
M9	-$(CH_2)_2$ [M-H]-	$C_{12}H_{16}N_4O_2$	247.1207	2.7	8.04	6.07E + 05
M21	-$C_6H_4N_4$+Glucuronidation [M-H]-	$C_{14}H_{24}O_8$	319.1389	−2.8	8.27	1.80E + 05
M22	Glucuronidation [M-H]-	$C_{20}H_{28}N_4O_8$	451.1822	−2.7	8.31–8.64	3.43E + 05
M23	-$C_6H_4N_4$+Glucuronidation [M-H]-	$C_{14}H_{24}O_8$	319.1390	−2.8	8.56	8.28E + 04
M10	-$(CH_2)_2$+Methylation [M-H]-	$C_{13}H_{18}N_4O_2$	261.1358	0.3	8.67	1.12E + 05
M24	2x Methylation + Oxidation [M-H]-	$C_{16}H_{24}N_4O_3$	319.1777	0.3	8.74	1.92E + 05
M13	Ketone + Methylation [M-H]-	$C_{15}H_{20}N_4O_3$	303.1466	1.1	9.12	2.23E + 05
M15	Desaturation [M-H]-	$C_{14}H_{18}N_4O_2$	273.1368	4.0	10.12	3.53E + 04
M25	Unassigned +102.0212	Unassigned	377.1726	N/A	10.44	5.70E + 05
M16	2x Methylation [M-H]-	$C_{16}H_{24}N_4O_2$	303.1823	−1.0	10.52	4.49E + 05

M17, M18, and **M25**, all exhibiting gains in mass over the **Parent**, could not be assigned as MS/MS fragmentation was limited. All 20 metabolites identified in ESI^- mode and their assigned structures have been summarized in Table 3, with the corresponding MS/MS spectra provided in the Supporting Information.

Major urinary metabolites

Analysis of urine was performed on a limited bladder collection volume from the 24-hr necropsies, therefore, only the major metabolites are reported. A small amount of the **Parent** 8-BOA was excreted unchanged, with an average concentration of ~9 nM in the 24-hr urine. **M3**, the tetra-demethylenation product, was the major metabolite in ESI^+ mode, with matching retention time and fragmentation to that seen in plasma (Figure S5(A,C)). Using 8-BOA calibration standards, the average **M3** concentration was estimated to be ~400 nM (although due to a number of unknowns, this should not be regarded as a semi-quantitative concentration). **M21**, the acyl-glucuronide minus ABT, appeared to be the major metabolite in ESI^- mode, with matching retention time and fragmentation to that seen in plasma (Figure S5(B, D)). Again, **M21** may not be a unique metabolite in itself, but rather an artefact of in-source fragmentation.

Characterization of mechanism-based inactivation of CYP4Z1 by 6-BHA

Time- and concentration-dependent loss of CYP4Z1-mediated Luc-BE *O*-debenzylation activity was observed from treatment with 6-BHA (Figure S6), typical of MBIs. This resulted in inactivation kinetic parameters of K_I = 29 μM and k_{inact} = 0.19 min^{-1}.

Ex vivo analysis

Off-target CYP inactivation

To assess the degree of off-target CYP inactivation *in vivo* from 8-BOA treatment, liver and kidney microsomes prepared from both control and treated groups were used for *ex vivo* CO-binding experiments to quantify the total pool of CYP content. Pooled liver microsomes yielded values of 0.71 and 0.60 nmol/mg for the control and treated rats, respectively, equating to a ~15% decrease due to treatment with 8-BOA. No appreciable difference in kidney microsomal CYP content was evident, with concentrations equalling 0.13 and 0.14 nmol/mg for control and treated samples, respectively (Figure 5(A)).

Off-target CYP activity

As another measure of off-target inhibition, *ex vivo* analysis of midazolam 1′-hydroxylation (M1OH), dextromethorphan *O*-demethylation (DOD), and phenacetin *O*-deethylation (POD) activities was performed to assess CYP3A, −2 C, and −1 A activity, respectively, in liver microsomes derived from both control and treated groups. Rates of M1OH, DOD, and POD for control microsomes were 42.5 ± 1.0, 113 ± 0.7, and 31.0 ± 1.0 pmol/mg protein/min, respectively (average ± SD). Rates of M1OH, DOD, and POD for treated microsomes were 43.7 ± 2.0, 118 ± 6.0, and 26.8 ± 2.0 pmol/mg protein/min, respectively (Figure 5(B)). While no decreases in M1OH or DOD activity were evident, a minimal 8.6% decrease in POD activity (CYP1A) was observed.

Clinical chemistries

Standard markers of liver and kidney function were assessed in plasma for the vehicle control group and the 8-BOA treated group for both pre-infusion and 24 hr post-infusion timepoints. Most analytes changed very little between conditions, with the exceptions of glucose (GLU) and aspartate

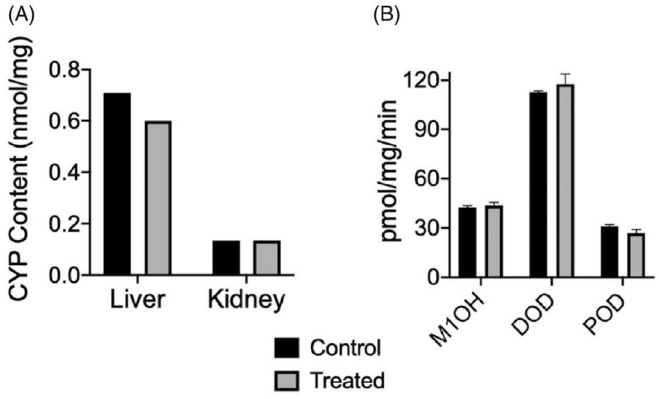

Figure 5. *Ex vivo* assessment of off-target CYP inactivation in rats treated with 8-BOA. Liver and kidney were harvested after 24 hours and microsomes were prepared from rats receiving either 8-BOA (treated, grey bars) or a vehicle infusion (control, black bars). CYP content from pooled microsomes was analysed *via* CO-binding difference spectra, where a ~15% decrease in liver microsomal CYP content was observed; no appreciable decrease in kidney microsomal CYP content was evident. Shown is the average from two replicates (A). Pooled liver microsomes derived from either control or treated animals were incubated with separate probe substrates in the presence of NADPH and rates of midazolam 1′-hydroxylation (M1OH), dextromethorphan *O*-demethylation (DOD), and phenacetin *O*-deethylation (POD) were determined. A ~9% decrease in POD activity was observed in the microsomes derived from treated compared to control animals, while no decreases in M1OH or DOD activity was evident. Shown is the average and standard deviation from three replicates (B).

Table 4. Kinetic parameters of CYP4Z1 inactivation for 8-BOA and 6-BHA.

Parameter	8-BOA	6-BHA (M9)
K_I (μM)	2.2[a]	29
k_{inact} (min^{-1})	0.15[a]	0.19
k_{inact} /K_I (min^{-1} μM^{-1})	6.8E-2	6.5E-3
fu	0.02	0.25
$K_{I,\ fu\ adjusted}$ (μM)	110	116
k_{inact} /$K_{I,\ fu\ adjusted}$ (min^{-1} μM^{-1})	1.4E-3	1.6E-3

Shown are the averages from technical replicates ($n = 3$)
[a]Determined from a previous study (Kowalski et al., 2020)

aminotransferase (AST). Control and treated groups both saw ~2.7-fold decreases in GLU, and 2.0- and 1.7-fold increases, respectively, in AST levels from pre-infusion to 24-hr. Therefore, no indication of acute toxicity arising from treatment with the test article is evident, as the increased AST levels are likely from the vehicle formulation that was used. The results for all analytes, groups, and timepoints are summarized in Table S1.

Simulated in vivo CYP4Z1 inhibition

The 8-BOA time – plasma concentration profile from the current study was used to simulate the effect this inhibitor would have on CYP4Z1, if it were expressed in a highly perfused xenografted tumour in the rat. Using constants obtained *in vitro* to characterize the inactivation kinetics of 8-BOA towards CYP4Z1 (*i.e.*, K_I and k_{inact}), the percent of active CYP4Z1 enzyme remaining after exposure to this inactivator (over time) was modelled from time 0 (pre-dose) to 96-hr post dose. From a starting point of 100% at time 0, the lowest values of percent active CYP4Z1 remaining were modelled to occur at 1.25, 1.5, and 2.25 hr and were 18, 16, and 15% for the scenarios corresponding to a $t_{1/2,\ CYP}$ of 1, 2, and 4 days, respectively. Values at 24 hours post-treatment were 55, 37, and 23% for $t_{1/2,\ CYP}$ of 1, 2, and 4 days, respectively. After 96 hr, values were 95, 78, and 49% for $t_{1/2,\ CYP}$ of 1, 2, and 4 days, respectively (data not shown).

Discussion

We recently designed and characterized 8-BOA as a selective, and mechanism-based inhibitor of mammary-restricted human CYP4Z1 (Kowalski *et al.* 2020). Through inhibition of this target enzyme, we could expect to lower production of its PUFA-derived pro-angiogenic metabolites (such as 14,15-EET), thereby potentially reducing the growth of metastatic breast cancer. However, detailed assessment of the inhibitor's *in vivo* pharmacokinetic characteristics is necessary to guide the design of CDX/PDX-rodent model experiments and to evaluate whether a prodrug approach or bioisosteric modifications would further lead compound optimization. The complexities surrounding pre-clinical models of breast cancer are well modelled in rats, and this species better mimics human physiology in comparison to mice (Smits *et al.* 2007, Iannaccone and Jacob 2009, Mollard *et al.* 2011). Therefore, the rat was used to capitalize on these aspects and, additionally, the practical considerations for this pilot study of enabling serial blood draws with a minimal number of animals.

Preliminary *in vitro* experiments assaying for metabolic stability of 8-BOA in liver and kidney microsomes (supplemented with co-factors to predict summative CYP- and UGT-mediated clearance) indicated the test article is a highly stable compound, as negligible depletion of 8-BOA was observed. We reasoned that this lack of depletion might be due to potent inactivation of rat CYP isoforms by this ABT analog. However, as evidenced by minimal inactivation of the general pool of rat liver microsomal CYPs following treatment with 100 μM of 8-BOA, this was clearly not the case *in vitro*. Therefore, we hypothesized that 8-BOA may either experience a prolonged half-life *in vivo or* be excreted substantially unchanged.

A single low dose of 10 mg/kg was chosen to avoid potential organ toxicities that might arise, as this was the first *in vivo* study for this new chemical entity. IV bolus administration was utilized to enable the highest potential plasma concentration as we were not concerned with oral bioavailability at this stage of interrogation. This produced a plasma C_{max} of 130 μM and a bi-phasic profile displaying a prolonged elimination $t_{1/2}$ of 6.1 hr. Although we cannot say at this time that 8-BOA would infiltrate into a tumour microenvironment directly, the high calculated V_z provides evidence that 8-BOA may penetrate tissues to a substantial extent. If future studies demonstrate that an increase in lipophilicity is required to raise tissue concentrations, esterification of the carboxylic acid may be an effective strategy. Lastly, a promisingly minimal *CL* value was observed; assuming that hepatic clearance dominates, the extraction ratio for 8-BOA in the rat is ~20%, binning into the 'low' category (Davies and Morris 1993, Rowland and Tozer 2011).

Scaling *in vitro* data for the prediction of drug-drug interactions due to mechanism-based inactivation of CYPs for

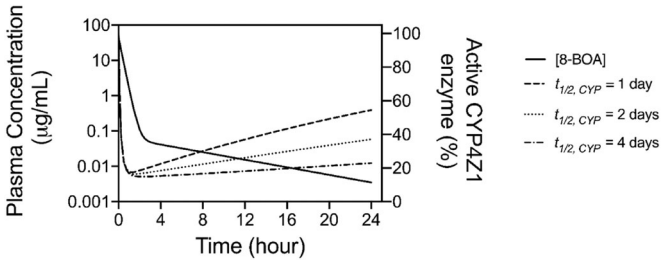

Figure 6. Simulation of active CYP4Z1 enzyme remaining (%) after treatment with the inhibitor 8-BOA, in a theoretical breast cancer xenograft model. Plasma concentrations of 8-BOA were calculated using the equation generated from the time-concentration profile of this study and the enzyme remaining after inactivation calculated from the unbound fraction of 8-BOA (2%) at these time points and the parameters $K_I = 2.2\,\mu M$ and $k_{inact} = 0.15\,min^{-1}$. The results from using different CYP turnover half-lives ($t_{1/2,\ CYP}$), ranging from 1–4 days, show that CYP4Z1 would remain 45–77% inactivated 24-hours post dose. [8-BOA] corresponds to the left axis, and the active CYP4Z1 enzyme remaining (%) for $t_{1/2,\ CYP} = 1$, 2, and 4 days corresponds to the right axis.

drug candidates has become common practice (Obach *et al.* 2007). We previously characterized the MBI parameters *in vitro* for the inactivation of CYP4Z1 by 8-BOA, resulting in a $K_I = 2.2\,\mu M$ and a $k_{inact} = 0.15\,min^{-1}$ (Kowalski *et al.* 2020). These values, taken together with the pharmacokinetic profile, allowed for an estimation of the potential CYP4Z1 inactivation that would occur in a xenograft model where the tumour expresses this enzyme. Contrary to an *in vitro* setting where the target enzyme can become virtually all depleted, *de novo* synthesis occurring *in vivo* will regenerate the enzyme pool concurrently. The turnover half-lives that have been determined for CYPs vary widely due to both isoform differences as well as the technically challenging, and indirect methods of measurement that are employed. As this information is clearly lacking for CYP4Z1, we used a $t_{1/2,\ CYP}$ range of 1–4 days to encompass the spectrum that has been reported for this constant (Zhang and Wong 2005, Yang *et al.* 2008). Furthermore, for this simple exercise, intratumoral exposure to the unbound fraction of 8-BOA (2%) was modelled as occurring in the central compartment, ignoring both the lag-time to reach a peripheral tumour, and the potential for the concentration to build inside the tumour.

The simulation in Figure 6 shows a rapid decline of active CYP4Z1 enzyme after exposure to inhibitor. This resulted in a nadir of 15–18%, suggesting CYP4Z1 activity would be decreased by 82–85%. After 24 hr, values for active CYP4Z1 remained <60%, indicating that all three $t_{1/2,\ CYP}$ scenarios result in prolonged CYP4Z1 inactivation from a single administration of 8-BOA. Therefore, given the relatively rapid and potent inactivation from 8-BOA and the time required for enzyme re-synthesis, maintaining constant high concentrations for reversible inhibition *in vivo* is not expected to be required for efficacy against the hypothesized pro-metastatic activity of CYP4Z1 (*i.e.,* as a 14,15-EET synthase).

Use of both ESI^+ and ESI^- modes in LC-MS/MS proved to be an effective strategy for metabolite identification as several metabolites were unique in their mode of ionization and fragmentation profile. While clearly there are ionization differences between metabolites, peak areas were used as a metric for qualitative comparisons of relative amounts as we lacked both a radiolabeled **Parent** and a majority of metabolite standards. We were particularly interested in assessing the circulating metabolites present in plasma for this pilot study to elucidate if any could contribute to either off- or on-target activity (Loi *et al.* 2013). Therefore, exploratory metabolite identification was performed with plasma pooled from the 5-min through 24-hr timepoints. Although a method such as described by Hamilton et al. using timepoint aliquots for an AUC-representative pool was considered (Hamilton *et al.* 1981), low available sample volumes necessitated the use of all available timepoints (particularly to acquire adequate signal intensity for diagnostic MS/MS fragmentation).

Analysis of pooled plasma in ESI^+ mode revealed 16 metabolites. The principal metabolite by peak area was **M9**, which showed a loss of $(CH_2)_2$ from the **Parent**. This metabolite, 6-BHA, was confirmed through matching retention times and MS/MS fragmentation to a chemical standard. By inspection of diagnostic fragmentation ions, the next largest metabolite **M3,** was assigned as the further chain-shortened 4-BBA, a total loss of $(CH_2)_4$ from the **Parent**. The presence of **M3** and **M9** provide strong evidence that β-oxidation of 8-BOA is a major pathway of metabolism in the current study and may largely explain the discrepancy between microsomal *in vitro* and *in vivo* half-lives. It also seems likely that the desaturation, mono-oxidation, and ketone formation metabolites that were also identified may be intermediate products from β-oxidation according to the 'leaky hosepipe' theory for this pathway (Stewart et al. 1973, Stanley and Tubbs 1975). The presence of **M19** as a hydroxylated variant of **M9**, and **M1** as the carnitine-conjugate of **M3**, are additional markers for β-oxidation (Figure 7); both mitochondria and peroxisomes could conceivably be the sites of this biotransformation (Suga 2003). It should be noted that the multiplicity of isomers for desaturation, mono-oxidation, and ketone formation metabolites certainly suggests contributions from other sources of metabolism as well. Retrospective analyses of metabolites formed from *in vitro* microsomal incubations, compared to plasma metabolites, may be helpful in delineating between potential intermediate β-oxidation versus CYP products in future studies. The use of additional *in vitro* matrices for metabolite identification and comparison, such as hepatocytes and S9 fractions, would also be helpful experiments to perform for further interrogation.

Analysis of pooled plasma in ESI^- mode revealed many of the same metabolites as seen in ESI^+ and again, **M3** and **M9** were majorly represented. As expected, the metabolite profile was increased and totalled 25 between the two modes of ionization, with glucuronide conjugates being newly revealed. **M20** at 7.8 min, and **M22**, denoting the cluster of peaks from 8.3 to 8.6 min, showed fragmentation indicative of acyl-glucuronides. These likely represent a mixture of the 1-β anomer as well as the 2-, 3- and 4-α/β acyl-glucuronide anomers akin to that seen in mouse metabolism of diclofenac (Sarda *et al.* 2012). Furthermore, **M21** and **M23** were identified as ions with fragmentation indicating that they were acyl-glucuronide structures that had lost their ABT

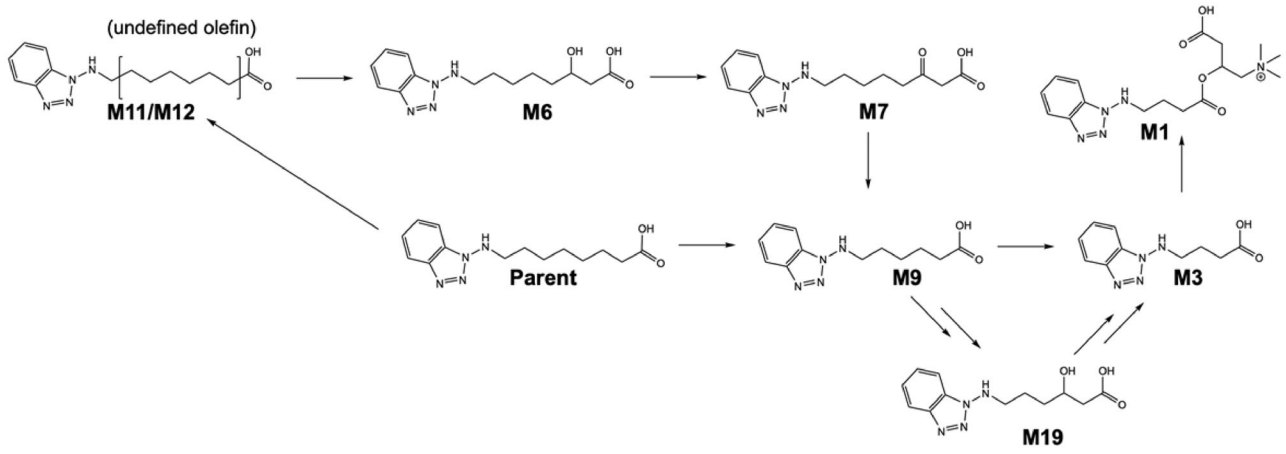

Figure 7. Structures of proposed metabolites in pooled plasma that provide evidence for the β-oxidation pathway. Successive removal of $(CH_2)_2$ generates **M9** (6-BHA, confirmed through comparison to the chemical standard) and then **M3** (tentatively assigned as 4-BBA) from the **Parent** 8-BOA, typical metabolites expected from β-oxidation. The desaturations, hydroxylation, and ketone formation compounds, **M11/M12**, **M6,** and **M7**, respectively, may be products due to 'intermediate leakage' from the β-oxidation pathway. The presence of **M19** as a β-hydroxylated variant of **M9**, and **M1** as the carnitine-conjugate of **M3**, are additional markers for this route of metabolism. The presence of multiple isomers of several of the metabolites is evidence that they are also derived from other (most likely CYP) biotransformation pathways.

moiety. These metabolites had overlapping retention times with the presumed acyl-glucuronide cluster and therefore may be artifactually generated *via* in-source fragmentation of **M22** or sample work-up. Regardless, acyl-glucuronidation was identified as an additional biotransformation pathway for 8-BOA.

For ABT itself, the *N*-acetylated and *N*-glucuronidated products are the major metabolites that have been identified in rats (Ortiz de Montellano 2018). We were unable to find these metabolites, although **M24**, corresponding to the product of bis-methylation plus oxidation, could conceivably be due to acetylation on the exocyclic nitrogen followed by reduction, but MS/MS fragmentation was inconclusive. Seemingly, the flux towards biotransformation pathways targeted to the alkyl-carboxylic acid dominate over pathways targeted to the ABT moiety. Along with the products from CYP-mediated oxidation, metabolites that were identified in both modes of ionization included numerous methylated species and unassigned adducts that possessed both more or less hydrophobicity than the **Parent** (as discerned through retention times).

Analysis of urine was performed only on samples obtained during the terminal 24-hour necropsy, and therefore, conclusions drawn from its analysis are limited. Nevertheless, the major urinary metabolites by peak area in ESI^+/ESI^- provided further evidence for two of the main pathways of metabolism observed from plasma analysis. **M3**, assigned as 4-BBA, was the most dominant metabolite identified in ESI^+ mode with an estimated concentration of ~400 nM. As a comparison, the concentration of unchanged 8-BOA in the urine at the 24-hr collection was <10 nM. No metabolite pertaining to a full 8-BOA structure conjugated to a glucuronide (such as **M20** or **M22**) was detected in urine in ESI^- mode. However, the major metabolite identified was **M21** (exhibiting the same retention time and MS/MS fragmentation as that found in plasma), but again this metabolite may be artifactual.

A notable drug example of β-oxidation metabolism occurs with the class of 3-Hydroxy-3-methylglutaryl-CoA reductase inhibitors, referred to as the 'statins' (Li *et al.* 2006). At least in the case of lovastatin, the chain-shortened pentanoic acid derivative does not maintain any inhibitory activity towards its target enzyme (Vyas *et al.* 1990). Serendipitously, 6-BHA, the confirmed identity of the metabolite **M9**, had already undergone in-depth characterization as it was part of our congeneric series of analogs and showed promise as a CYP4Z1 MBI itself. 6-BHA exhibited a robust level of time-dependent inhibition while maintaining a similar degree of low off-target inhibition of human CYPs (Kowalski *et al.* 2020). Therefore, the plasma concentrations of 6-BHA were also determined and pharmacokinetic parameters for this metabolite were derived (Table 1). A rapid T_{max} of 0.14 hr indicates 8-BOA undergoes quick biotransformation to 6-BHA and the elimination $t_{1/2}$ for 6-BHA shows rapid flux to secondary metabolites such as 4-BBA. While it may be true that the rate constant for 6-BHA metabolism is more rapid than that of its formation from 8-BOA, according to metabolite kinetics logic, the terminal $t_{1/2}$ of the metabolite cannot be faster than the parent (Houston 1981). Therefore, it is likely that the terminal elimination phase was not fully characterized. Regardless, it is evident that in this scenario 6-BHA elimination should be considered as formation rate limited.

Although exhibiting a weaker affinity for CYP4Z1 (K_I > 10-fold higher), the k_{inact} determined for 6-BHA shows a similarly quick rate of CYP4Z1 inactivation to that of 8-BOA, 0.19 and 0.15 min^{-1}, respectively. Additionally, the lowered PPB exhibited by 6-BHA, 75% versus 98% for 8-BOA, suggests that free concentrations of this metabolite are likely to be more elevated *in vivo*. Taken together, a comparison of the 8-BOA and 6-BHA $k_{inact}/K_{I,}$ ($min^{-1}\,\mu M^{-1}$) ratios adjusted for PPB indicates comparable mechanism-based inactivation of CYP4Z1 could occur *in vivo* (outlined in Table 4). Therefore, it is tempting to speculate that the β-oxidation of 8-BOA may serve to augment the desired pharmacodynamic effect of

CYP4Z1 inactivation through the generation of an active metabolite *in vivo*. Future studies may characterize the inhibitory potency and PPB of 4-BBA and also dose 6-BHA itself to assess whether higher plasma exposure can be obtained with this analog instead.

The control arm group of the study enabled *ex vivo* assessment of liver and kidney CYP content/activity as well as clinical chemistries to evaluate acute toxicity. Given that 8-BOA showed heightened CYP4Z1-selectivity for time-dependent inhibition, we decided to limit our assessment to the proclivity for off-target CYP inactivation to occur in the rat. The observed ~15% decrease in the CYP content in liver microsomes derived from the treated animals, where a C_{max} of 130 μM was determined, is in good agreement with our *in vitro* analysis that showed 7% off-target CYP inactivation from treatment with 100 μM of 8-BOA. Taken together, these data demonstrate a relatively low propensity for 8-BOA to target hepatic CYP isozymes in the rat.

Although no truly isozyme-specific probe substrates have been described for rat liver CYPs, multiple studies have used semi-selective metabolism of probe substrates (the minor metabolizing isozymes are noted in parenthesis): M1OH to assess CYP3A1 and -3A2 (-C11, -C13), DOD to assess CYP2C6 and -2C11 (-2D2), and POD to assess CYP1A2 (-2C6) (Kobayashi *et al.* 2002, Chovan *et al.* 2007). Therefore, M1OH was used to probe residual CYP3A activity, DOD to probe CYP2C activity, and POD to probe CYP1A activity *ex vivo* in rat liver microsomes, A ~9% decrease in POD activity was observed in the microsomes derived from treated compared to control animals, while no decreases in M1OH or DOD activity was evident. Our previous characterization of 8-BOA inactivation of off-target human CYP isoforms showed that CYP1A2 experienced the largest degree of time-dependent inhibition, characterized by IC_{50} and shifted-IC_{50} values of 614 and 55 μM, respectively, equating to a shift ratio of 11. Since rat liver POD activity is driven mainly by CYP1A2, the minor ~9% decrease in treated versus control microsomes agrees with human CYP isozyme data. This indicates that while overall a minor process, CYP1A family enzymes may experience the largest off-target CYP inactivation liability from 8-BOA in both the human and rat.

Lastly, the results of clinical chemistries indicated that 8-BOA treatment causes no acute liver or kidney toxicity. Given that ABT, the bioactivatable pharmacophore of 8-BOA, has been itself dosed to numerous species and causes little toxicity (Ortiz de Montellano 2018), this is not a surprising result. While the potential for acyl-glucuronides to covalently modify proteins is well known (Faed 1984, Regan *et al.* 2010), xenobiotic fatty acids also can interfere with lipid metabolism. This can lead to their incorporation into triglycerides, the reduction of carnitine levels, and inhibition of β-oxidation, which can all trigger toxicological effects (Darnell and Weidolf 2013). At least in the short time scale of this study (and low dose), no indication of interference with these systems was apparent based on the results of the liver and kidney function tests. Of note, both control and treated groups showed a significant increase in aspartate aminotransferase (AST) levels from pre-infusion to the 24-hr timepoint; this was likely due to the infusion formulation that was utilized.

In summary, the IV pharmacokinetic profile of 8-BOA in the rat was defined by low *CL* and extended plasma exposure suggestive of pharmacodynamic efficacy in an appropriate pre-clinical model. Metabolite identification revealed β-oxidation as a major biotransformation pathway, which produced a circulating metabolite (6-BHA) that displays rapid mechanism-based inhibition of CYP4Z1. *Ex vivo* analysis showed only minor inactivation of off-target rat CYPs, matching that seen previously with human CYP isozymes. No indication of acute toxicity was observed. Therefore, this *in vivo* characterization of the inhibitor 8-BOA in rats suggests that we could appropriately interrogate the role of CYP4Z1 in breast cancer in a xenograft tumour model.

Acknowledgements

The authors thank Dale Whittington and Dr. J. Scott Edgar for mass spectrometry assistance and Dr. Brian Baer for useful drug metabolism discussions. The authors recognize Dr. Ellen Joy Plein, who throughout a long career contributed greatly to the University of Washington School of Pharmacy. The Plein endowed funds that were established have enabled many research opportunities, including the study presented here.

Disclosure statement

The authors report no conflict of interest.

ORCID

John P. Kowalski http://orcid.org/0000-0002-0343-8425

References

Al-Esawi N.S.E., *et al.*, 2020. Expression of CYT4Z1 in breast carcinoma; Correlating with clinicopathological parameters. *Biomedical and pharmacology journal*, 13:1.

Campbell, C.D., and Rees, C.W., 1969. Reactive intermediates. Part I. Synthesis and oxidation of 1- and 2-aminobenzotriazole. *Journal of the chemical society*, (5):742–747.

Capper, C.P., *et al.*, 2016. The Metabolism, analysis, and targeting of steroid hormones in breast and prostate cancer. *Hormones and cancer*, 7: 149–164.

Chovan, J.P., *et al.*, 2007. Cytochrome P450 probe substrate metabolism kinetics in Sprague Dawley rats. *Xenobiotica*. 37:459–473.

Darnell, M., and Weidolf, L., 2013. Metabolism of xenobiotic carboxylic acids: focus on coenzyme A conjugation, reactivity, and interference with lipid metabolism. *Chemical research in toxicology*, 26:1139–1155.

Davies, B., and Morris, T., 1993. Physiological parameters in laboratory animals and humans. *Pharmaceutical research*, 10:1093–1095.

DeSantis, C.E., *et al.*, 2019. Breast cancer statistics, 2019. *CA: A cancer journal for clinicians*, 69(6):438–451.

Faed, E.M. 1984. Properties of acyl glucuronides: implications for studies of the pharmacokinetics and metabolism of acidic drugs. *Drug metabolism reviews*, 15:1213–1249.

Guengerich, F.P., *et al.*, 2009. Measurement of cytochrome P450 and NADPH-cytochrome P450 reductase. *Nature protocols*, 4:1245–1251.

Hamilton, R.A., *et al.*, 1981. Determination of mean valproic acid serum level by assay of a single pooled sample. *Clinical pharmacology & therapeutics*, 3:408–413.

He, D., *et al.*, 2019. A novel immunodeficient rat model supports human lung cancer xenografts. *The FASEB journal*, 33:140–150.

Houston, J.B., 1981. Drug metabolite kinetics. *Pharmacology & therapeutics*, 15(3):521–552.

Iannaccone, P.M., and Jacob, H.J., 2009. Rats! *Disease models & mechanisms*, 2(5-6):206–210.

Kobayashi, K., *et al.*, 2002. Substrate specificity for rat cytochrome P450 (CYP) isoforms: screening with cDNA-expressed systems of the rat. *Biochemical pharmacology*, 63:889–896.

Kowalski, J.P., *et al.*, 2020. Design and characterization of the first selective and potent mechanism-based inhibitor of cytochrome P450 4Z1. *Journal of medicinal chemistry*, 63(9):4824–4836.

Li, C., *et al.*, 2006. Acyl-coenzyme a formation of simvastatin in mouse liver preparations. *Drug metabolism and disposition*, 34:102–110.

Li, Y., *et al.*, 2017. Tumoral expression of drug and xenobiotic metabolizing enzymes in breast cancer patients of different ethnicities with implications to personalized medicine. *Scientific reports*, 7:4747.

Loi, C.M., *et al.*, 2013. Which metabolites circulate? *Drug metabolism and disposition*, 41:933–951.

McDonald, M.G., *et al.*, 2017. Expression and functional characterization of breast cancer-associated cytochrome P450 4Z1 in Saccharomyces cerevisiae. *Drug metabolism and disposition*, 45:1364–1371.

Mollard, S., *et al.*, 2011. How can grafted breast cancer models be optimized? *Cancer biology & therapy*, 12:855–864.

Murayama, T., and Gotoh, N., 2019. Patient-derived xenograft models of breast cancer and their application. *Cells*, 8(6):621.

Murray, G.I., *et al.*, 2010. Profiling the expression of cytochrome P450 in breast cancer. *Histopathology*, 57:202–211.

Noto, F.K., *et al.*, 2018. Sprague dawley Rag2-null rats created from engineered spermatogonial stem cells are immunodeficient and permissive to human xenografts. *Molecular cancer therapeutics*, 17: 2481–2489.

Obach, R.S., *et al.*, 2007. Mechanism-based inactivation of human cytochrome p450 enzymes and the prediction of drug-drug interactions. *Drug metabolism and disposition*, 35:246–255.

Ortiz de Montellano, P.R., 2018. 1-aminobenzotriazole: a mechanism-based cytochrome P450 inhibitor and probe of cytochrome P450 biology. *Medicinal chemistry*, 8(3):038.

Radvanyi, L., *et al.*, 2005. The gene associated with trichorhinophalangeal syndrome in humans is overexpressed in breast cancer. *Proceedings of the national academy of sciences of the United States of America*, 102: 11005–11010.

Regan, S.L., *et al.*, 2010. Acyl glucuronides: the good, the bad and the ugly. *Biopharmaceutics & drug disposition* . 31:367–395.

Rieger, M.A., *et al.*, 2004. Identification of a novel mammary-restricted cytochrome P450, CYP4Z1, with overexpression in breast carcinoma. *Cancer research*, 64:2357–2364.

Rowland, M., and Tozer, T., 2011. *Clinical pharmacokinetics and pharmacodynamics: Concepts and Applications*. 4th ed. Philadelphia: Wolters Kluwer Health/Lippincott Williams & Wilkins.

Sadeque, A.J., *et al.*, 1992. Stereoselective sulfoxidation by human flavin-containing monooxygenase. Evidence for catalytic diversity between hepatic, renal, and fetal forms. *Drug metabolism and disposition*, 20: 832–839.

Sarda, S., *et al.*, 2012. Diclofenac metabolism in the mouse: novel in vivo metabolites identified by high performance liquid chromatography coupled to linear ion trap mass spectrometry. *Xenobiotica*. 42: 179–194.

Smits, B.M., *et al.*, 2007. Genetically engineered rat models for breast cancer. *Breast disease*, 28:53–61.

Stanley, K.K., and Tubbs, P.K., 1975. The role of intermediates in mitochondrial fatty acid oxidation. *Biochemical journal*, 150:77–88.

Stewart, H. B., *et al.*, 1973. Intermediates in fatty acid oxidation. *Biochemical journal*, 132:61–76.

Suga, T., 2003. Drug metabolism in peroxisomes: involvement of peroxisomal beta-oxidation system in the oxidative chain-shortening of xenobiotic acyl compounds. *Drug metabolism and pharmacokinetics*, 18:155–162.

Vyas, K.P., *et al.*, 1990. Biotransformation of lovastatin. I. Structure elucidation of in vitro and in vivo metabolites in the rat and mouse. *Drug metabolism and disposition*, 18:203–211.

Yang, J., *et al.*, 2008. Cytochrome p450 turnover: regulation of synthesis and degradation, methods for determining rates, and implications for the prediction of drug interactions. *Current drug metabolism*, 9: 384–394.

Yang, X., *et al.*, 2017. CYP4Z1 - a human cytochrome P450 enzyme that might hold the key to curing breast cancer. *Current pharmaceutical design*, 23:2060–2064.

Zhang ZY and Wong YN. 2005. Enzyme kinetics for clinically relevant CYP inhibition. *Current drug metabolism*, 6:241–257.